Reaction with hot air of high entropy alloys strengthened by monocarbides formed from heavy metals: assessment of the oxidation kinetics from the analysis of the chemically changed subsurfaces

Patrice Berthod

RESEARCH ARTICLE

Asian Research Association

BULLETIN OF SCIENTIFIC RESEARCH

DOI: 10.54392/bsr2322

Reaction with hot air of high entropy alloys strengthened by monocarbides formed from heavy metals: assessment of the oxidation kinetics from the analysis of the chemically changed subsurfaces

Patrice Berthod [1, *]

[1] Institut Jean Lamour, Université de Lorraine, Nancy, 54000, France
*Corresponding author Email: patrice.berthod@univ-lorraine.fr
DOI: https://doi.org/10.54392/bsr2322
Received: 15-05-2023; Accepted: 18-11-2023; Published: 23-11-2023

Abstract: As in classical superalloys based on nickel or cobalt, MC carbides can be easily obtained in cast high entropy alloys (HEA) for enhancing their mechanical properties at high temperatures. These carbides may have also some influence on the hot oxidation properties. They can be also not neutral for the oxidation behavior. To explore their possible influence in this field, an equimolar CoNiFeMnCr reference alloy and two versions containing TaC or HfC carbides were prepared by casting and exposed to air at 1000°C. Their oxidation behaviors were studied by characterizing the obtained corrosion products and the modifications induced in the subsurfaces of the samples. Results show that TaC and HfC are moderately involved in the oxidation phenomena but they obviously influence the Cr and Mn diffusion toward the oxidation front. This seemingly aggravates more the already poor oxidation high temperature resistance of the base alloy. However the harmful effect of the TaC seems to be much lower than the one of the HfC, and the TaC–strengthened CoNiFeMnCr alloy is only a little less resistant against oxidation than the carbide–free reference equimolar alloy.

Keywords: High entropy alloys, Tantalum monocarbides, Hafnium monocarbides, High temperature exposure to air, Metallographic characterization, Hf-doping, Oxidation kinetic assessment

1. Introduction

The needs of high performance coarse–grained metallic materials, for fabricating complex–shaped components working at high temperature, stay important despite the progress of additive manufacturing. For achieving mechanical properties high enough at temperatures close to 1000°C and sometimes beyond, great grain size and dendritic coarseness are to be preferred. This is one of the reasons of the presence of Single–Crystalline (SX) or Directionally Solidified (DS) superalloys in the hottest zones of turbines (e.g. static and mobile blades) or glass–making (e.g. spinners) processes. The potential weak points of polycrystalline SD or equiaxed alloys are the grain boundaries (GB) and the interdendritic spaces (IS), from that the presence of strengthening phases in these areas. Among these particles allowing the reinforcement of GB and IS there are carbides. These ones can be of various types but, among the most efficient ones in this role, there are monocarbides formed by involving selected carbide–forming elements as Ta or Nb, and even Hf and Zr. All these metals [1] are able to form an interdendritic and intergranular network of MC carbides which enhance the high temperature mechanical properties, static tensile strength and creep resistance [2-4]. To push further the high temperature mechanical resistance working on the matrix is complementary. Indeed, matrix is generally the main from several decades this classically done by solid solution strengthening (substitutional heavy atoms dispersed in solid solution) or by hard particles precipitation (secondary carbides, intermetallic precipitates, dispersoids). One can also imagine to apply the base principle of the High Entropy Alloys (HEA) [5] to the austenitic matrixes of cast polycrystalline MC–reinforced superalloys, by replacing the Ni(Al) or Co(Cr) austenitic solid solutions by a mix, in similar proportions, of several metals chosen among Co, Cr, Cu, Fe, Mn, Ni … Despite HEAs exist since already several decades ago [6], this seems to do not have been tested until very recently. If this is really the case, the alloys resulting from the association of the well–known equimolar CoNiFeMnCr composition [7–10] with primary TaC or HfC, elaborated and microstructurally characterized [11,12] are possibly the first specimens of this family to have been considered. The Co–Ni–Fe–Mn–Cr system was among the early first HEAs to be studied and extensive investigations were carried out concerning them, in the fields of

thermodynamic [13], magnetic [14], diffusion behavior [15] or strengthening [16,17]. This alloy was logically chosen to test, in a first time if this was possible to obtain TaC or HfC carbides similar to the ones strengthening cobalt–based or nickel–based alloys efficiently [2,3], and in a second time to check whether the presence of these carbides really brought significant reinforcement to equimolar CoNiFeMnCr alloy. These tests confirmed that script–like eutectic TaC [11] or HfC [12] carbides were successfully obtained in the spaces separating grains and the ones separating the dendrites of matrix from one another, and that the creep resistance at high temperature was really enhanced by their presence [18].

One of the other most important properties for alloys developed for applications inducing elevated working temperatures is the resistance against oxidation. Equimolar CoNiFeMnCr alloys containing TaC or HfC may present potential problems in this field, for several reasons. First, the equimolar principle automatically limits the Cr content to around 20 wt.%, which is in the bottom side of the Cr content range usually respected for chromia–forming high temperature alloys or superalloys. Second, particles rich in Ta or Hf (which are highly oxidable metals), furthermore located in the grain and interdendritic boundaries (which are zones known to be high diffusion pathways for the species involved in the oxidation phenomena), may degrade the oxidation behavior.

A series of investigations were already carried about the behavior of HEAs in high temperature oxidation. Among the studied alloys which are the closest to the Cantor composition but which are slightly different, there are Mn–free Al–containing ones (AlCoCrFeNi) [19,20], or some Ni–free ones [21,22], for instance. The oxidation behavior of the equimolar CoNiFeMnCr composition was specifically investigated in laboratory air at temperatures from 500°C to 900°C [23,24], and in synthetic air between 900 and 1100°C [25]. In this later study, it was notably observed that Cr and Mn had the most important roles in the oxidation process; after 24 hours of oxidation they were particularly present in the external and internal corrosion products (Mn_3O_4, $(Mn,Cr)_3O_4$ and Cr_2O_3.

The purpose of this work is to explore the oxidation behavior of the matrix and of the whole alloys in air at 1000°C during 50 hours, and compare them to alloys containing only a single base element (Ni, or Co, or Fe). These investigations concern then: an equimolar CoNiFeMnCr alloy (named “CTR alloy”) with comparison with Co(Cr) and Ni(Cr) alloys, and a CTR alloy added with TaC, and another one added with HfC, with comparison with Co(Cr)+TaC or HfC, Ni(Cr)+HfC and Fe(Cr)+HfC at similar temperatures.

2. Materials and Methods

2.1 Preparation of the alloys for the study

Three alloys were obtained as 40g–weighing ingots by melting pure elements (Alfa Aesar, purity > 99.9%) together and by solidifying the liquid melts in inert atmosphere conditions. Their chemical compositions were initially chosen among the ones earlier investigated to explore the as–cast microstructures of such MC–added HEA alloys [11,12]. They are here: the CoNiFeMnCr (→ “HEA”) equimolar composition, the same composition with tantalum (Ta) and carbon (C) additions defined to obtain 0.25 wt.% of C and 3.7wt.% of Ta (→ “HEA-t”), and the same composition again but with hafnium (Hf) instead tantalum, and carbon (C) additions to reach 0.25 wt.% C and 3.7wt.% Hf (→ “HEA-h”). The accurately weighted (balance with a 0.1 mg precision) mix of pure elements was placed in the water–cooled copper crucible of a high frequency induction furnace. The fusion chamber was isolated from outside by a silica tube. The laboratory air was removed by pumping, and replaced by pure argon (300 mbars). Heating, melting, liquid state chemical homogenization were produced by generating a 100 kHz alternative current (maximal voltage: 5 kV) in the coil surrounding the silica tube and the crucible containing the alloy.

2.2 Preparation of the samples

Each of the three ingots was cut to obtain two parts. One played the role of a metallographic sample allowing the examination of the as–cast microstructure and the control of the real chemical composition. The second one was destined to the oxidation test. The part for metallography was embedded in resin and ground (SiC papers from #240 to #1200) then polished (textile disk supporting hard micrometric particles). These mirror–like metallography samples were ready for controlling the microstructure, using a Scanning Electron Microscope (SEM JEOL JSM6010LA) in Back Scattered Electrons mode (BSE), as well as their chemical composition by Energy Dispersion Spectrometry (EDS). The oxidation test samples, 3 × 10 × 10 (mm) parallelepipeds, were ground with #1200 SiC papers on all their faces, and their edges and corners were smoothed using the same grinding papers.

2.3 Oxidation tests

The three oxidation test samples were layed on a ceramic flat support. This one was introduced in the hot central zone of a resistive furnace where temperature was rated at 1000°C. Here the samples stayed for 50 hours. At the end of this duration, the furnace was switched off and the samples cooled in the furnace (closed). After complete cooling the furnace

was opened. The oxidized samples were carefully handled for first the characterization of the oxidized surfaces X-Ray Diffraction (XRD). The used diffractometer was a Bruker D8 Advance model, using a Cu K_α radiation). Thereafter, the oxidized samples were embedded in resin and cut for obtaining cross–sectional metallographic samples. These ones were ground and polished to allow the observations and characterization with the same techniques as for the as–cast metallography samples (SEM, EDS).

3. Results and Discussion

3.1 Microstructures in the as-cast condition

The SEM/BSE micrographs given in Figure 1 allow observing that the state of the "HEA" alloy is seemingly single–phased and that the "HEA-t" and "HEA-h" are obviously double–phased (with bright particles identified by EDS as being MC carbides). The "HEA-t" alloy contains finely structured eutectic TaC carbides in great proportion, and also some coarser TaC. The carbides which can be seen in the "HEA-h" alloy are of two types too. One can distinguish eutectic HfC carbides and some HfC particles which are a little coarser than the previous ones. The chemical compositions of the alloys coming from EDS full frame analysis (performed on several x 250 areas) are close to the wished ones.

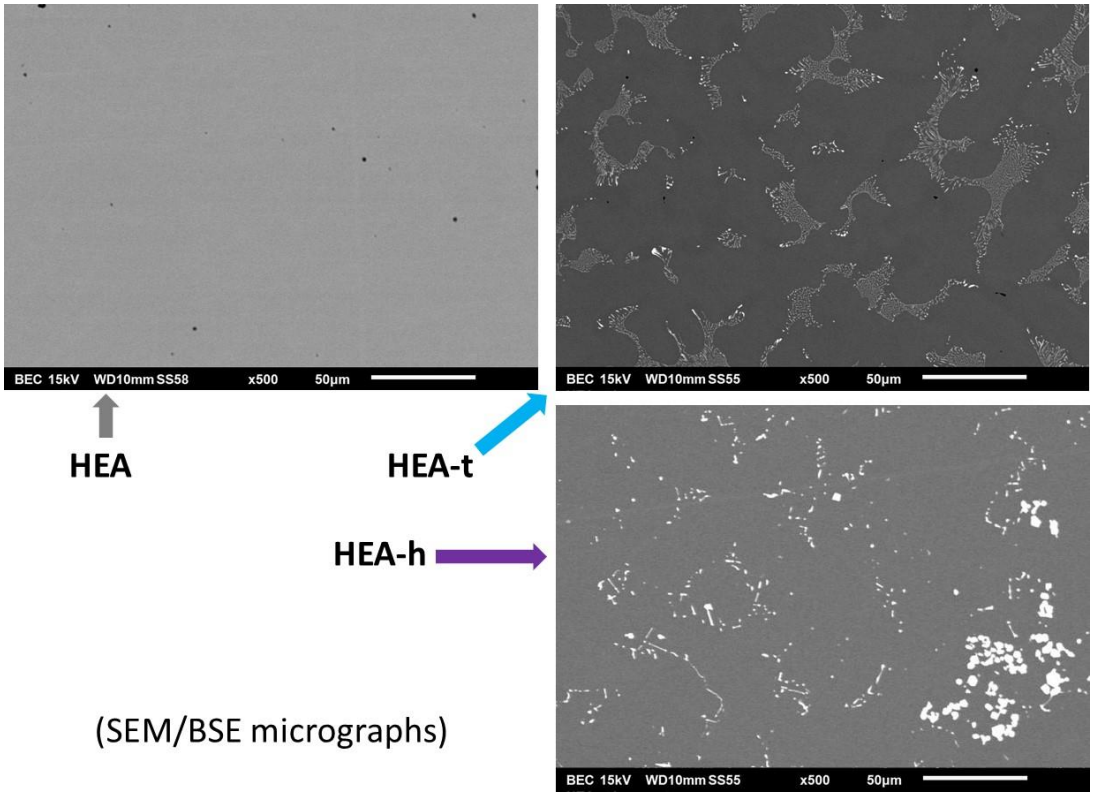

Figure 1. As-cast microstructure of the Ni-25Cr-4Ta-2Hf alloy." by "As-cast microstructures of the three studied alloys.

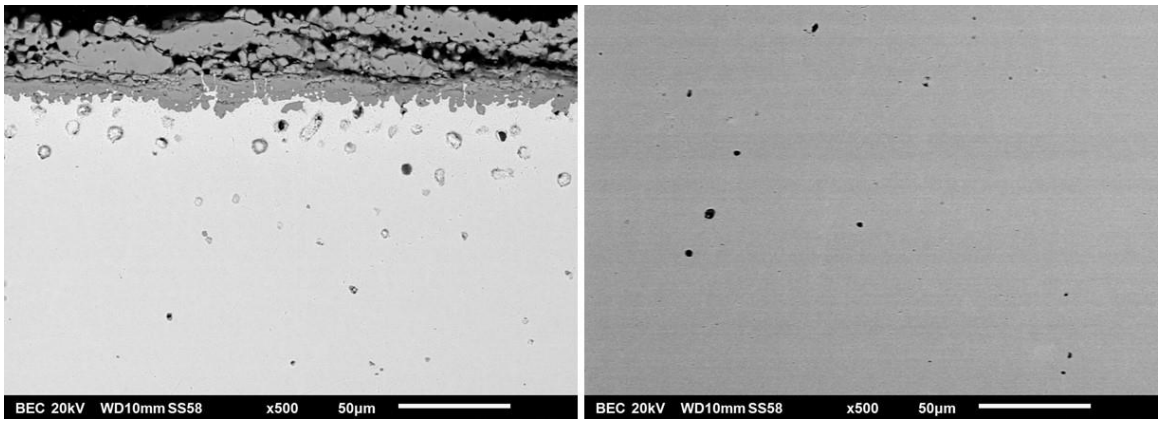

Figure 2. Oxidation state of the "HEA" alloy (left) and bulk state after 50h at 1000°C (right).

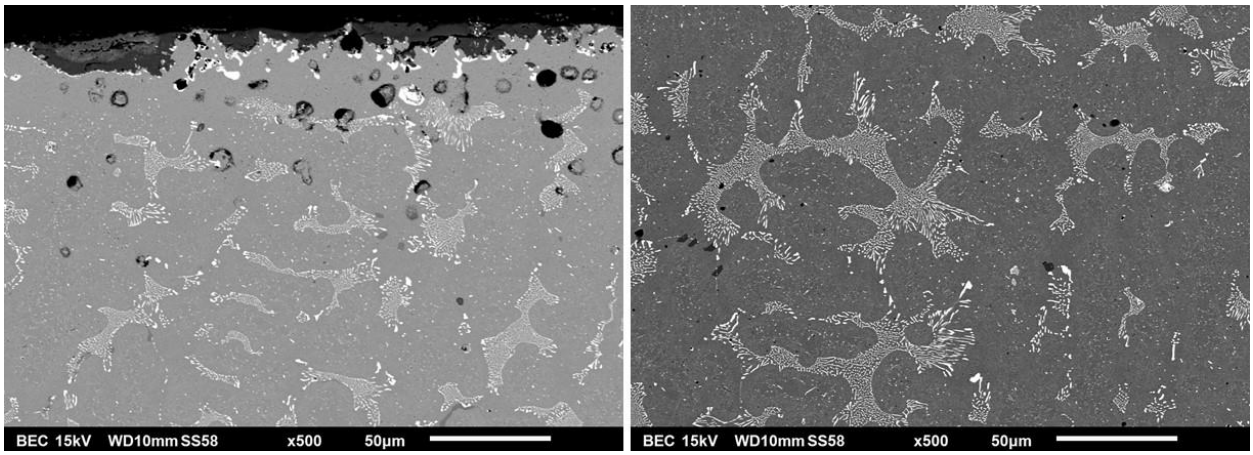

Figure 3. Oxidation state of the "HEA-t" alloy (left) and bulk state after 50h at 1000°C (right).

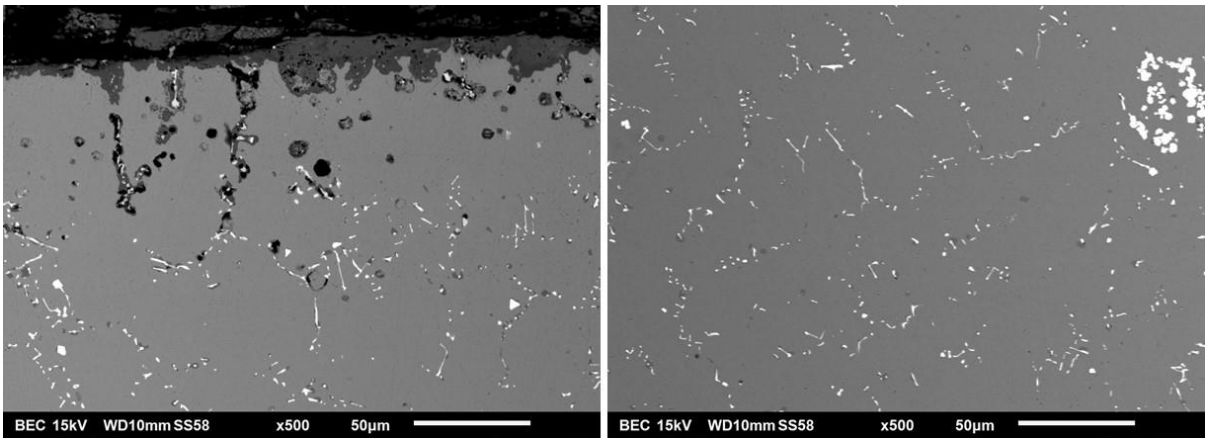

Figure 4. Oxidation state of the "HEA-h" alloy (left) and bulk state after 50h at 1000°C (right).

3.2 Oxidation state of the "HEA" alloy

Naked-eye and optical microscope observations evidenced that many parts of oxides were obviously lost during cooling. The SEM/BSE picture presented in Figure 2 (left) gives a view of the oxidized surface state: obviously the external oxide scale can be constituted of two superposed layers. The inner oxide layer, which is rather compact, seems having grown inwards, as suggested by the irregular penetration front of oxidation. This inner oxide part is globally still present all around the sample. The outer oxide scale is much more porous and it was obviously lost here and there during the post isothermal oxidation cooling. Observations at higher magnification allows seeing that the gray of oxide is of various levels in the oxide scale. EDS spot analysis shows that they are oxides of the M_3O_4–type (M = Mn and Cr with various relative proportions). Some oxide areas are very close to the spinel $MnCr_2O_4$ stoichiometry. One can also notice several isolated chromia oxides (Cr_2O_3): they are present at the frontier between the oxide scale and the alloy, principally. The natures of the observed oxides are in good agreement with what was earlier reported in papers dealing with the oxidation of equimolar CoNiFeMnCr alloys at temperature of about 1000°C for shorter durations (12h or 24h) [21, 24]. The presence of porosities in the subsurface let think to the Kirkendall pores formation induced by oxidation. The Kirkendall effect as well as the noticeable oxide spallation were reported in previous studies for induction cast CoNiFeMnCr equimolar alloys after oxidation at 1000°C [24].

In contrast with surface and subsurface, the fifty hours spent at 1000°C did not induce particular changes in the bulk (Figure 2, right).

3.3 Oxidation state of the "HEA-t" alloy

A part of the oxides developed on the surface of the "HEA-t" alloy spalled off during cooling, too. The SEM/BSE micrographs presented in Figure 3 (left) evidences that the oxide scale was, also here, made of an outer part (a great part of which lost by spallation), and of an inner part which was better kept by the alloy. As observed for the "HEA" alloy, the oxides rich in Cr are mainly close to the alloy and the ones rich in Mn are farer. The oxides involving tantalum are concentrated at the scale/alloy interface for some of

them, while other $CrTaO_4$ formed a little deeper in the subsurface. The Kirkendall phenomenon is visible over 50 µm from the scale/alloy interface. An additional phenomenon, by comparison to the "HEA" alloy is the obvious disappearance of the tantalum carbides in a 30–40 µm depth. Another difference: secondary fine TaC carbides precipitated in the matrix, deeper than this zone as well as everywhere in the bulk (Figure 3, right).

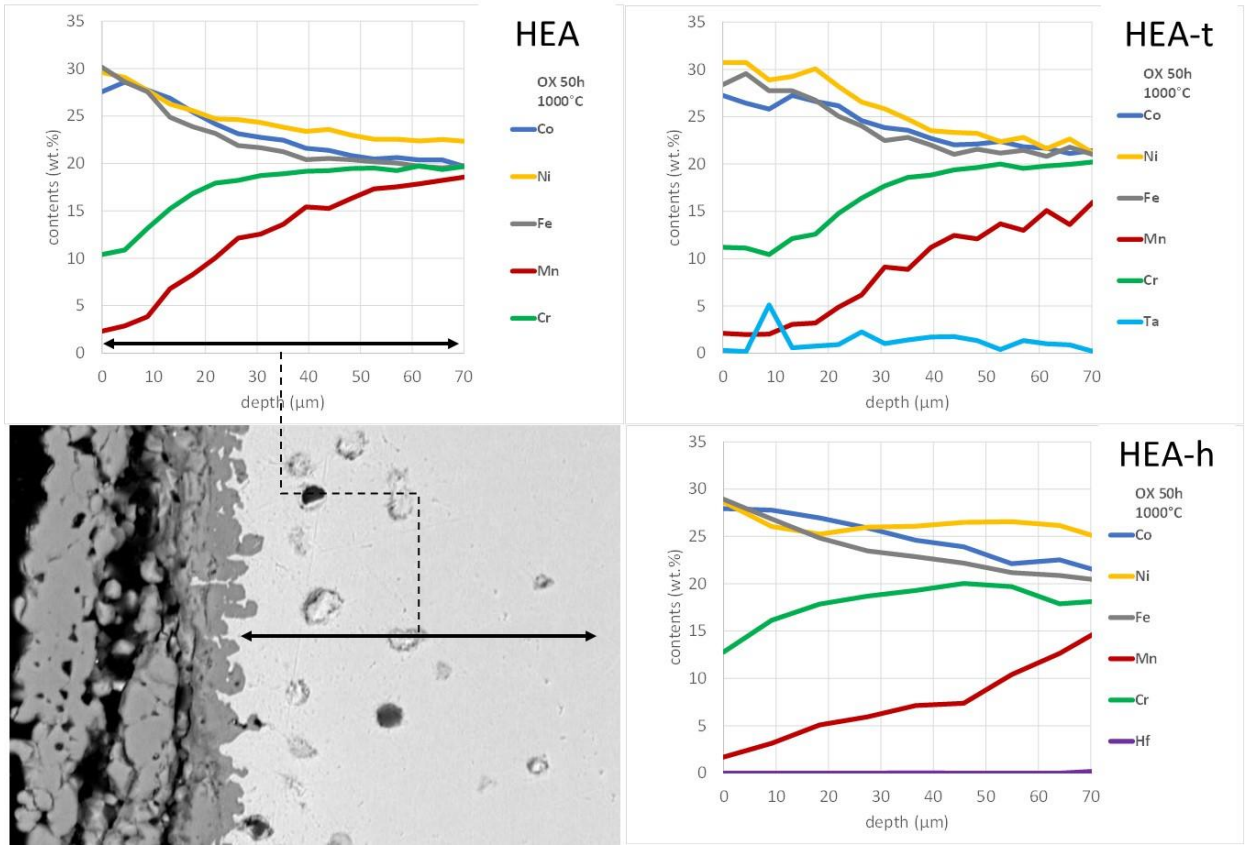

Figure 5. Elemental concentration profiles acquired in the oxidation–modified subsurfaces of the HEA alloy (top left, concerned zone as example: bottom left), of the HEA-t alloy (top, right) and of the HEA-h alloy (bottom right).

Table 1. Quantitative exploitation of the Cr–concentration profiles

Characteristics of Cr-depletion:	mini wt.% close to oxidation front	depletion depth (µm)	mass lost (g/cm^2)
HEA	7 - 11	50 - 70	0.001 – 0.002
HEA-t	10 - 11	50 - 60	0.001 – 0.002
HEA-h	5 - 13	40 - 70	0.001 – 0.003

Table 2. Quantitative exploitation of the Mn–concentration profiles

Characteristics of Mn-depletion:	mini wt.% close to oxidation front	depletion depth (µm)	mass lost (g/cm^2)
HEA	2 - 3	60 - 100	0.004 – 0.005
HEA-t	1 - 2	100 - 140	0.005 – 0.007
HEA-h	1 - 2	100 - 110	0.007 – 0.009

3.4 Oxidation state of the "HEA-h" alloy

SEM/BSE and EDS observation and characterization were also performed in the cross–sectional sample prepared from the oxidized "HEA-h" sample. The observed oxides are the same as for the reference "CTR" alloy, except a new oxide: HfO_2. Seemingly the "HEA-h" alloy was more degradated by oxidation than the two other alloys. There is notably a particularly deep internal oxidation in its case (Figure 4, left). The main part of oxide scale was again made of an outer part (here too partly lost by spallation during cooling) and an inner part with an irregular interface with the subjacent alloy. Along, the oxides are richer in Cr (Cr_2O_3 was notably found). The hafnium carbides close to the scale/alloy interface were internally oxidized, the eutectic ones as well as the pre–eutectic ones. Concerning the bulk of this third alloy, no noticeable phenomenon occurred (Figure 4, right).

3.5 Chemical changes in the subsurfaces of the three alloys

The formation of external and internal oxides was necessarily accompanied by chemical change in the alloys, more precisely in the regions close to the oxidation front. To discover these subcortical chemical changes a series of concentration profile were acquired in alloy perpendicularly to the external surface. Zoomed parts (over a depth limited to 70µm to better observe the evolution very close to the oxidation front) of the obtained concentration profiles are displayed in Figure 5. They evidence that this is in manganese that the subsurface is the most impoverished as a consequence of the oxidation of the alloys. In the total profiles one can also see that the Mn–depletion tends to be more extended than the Cr–depletion. In addition, the minimal content, visible at the {oxide scale / alloy} interface, is considerably lower for Mn than for Cr. Quantitative data relative to these observations are available in Table 1 (for Cr) and Table 2 (for Mn).

If results are compared among the three alloys, it additionally appears that the minimal Cr and Mn contents close to the oxidation front are lower for the HEA-t and HEA-h alloys than for the HEA alloy (Mn: true for the HEA-t and HEA-h alloys, Cr: true only for the HEA-h alloy). The depths depleted in Cr are almost the same for the three alloys but the depths depleted in Mn of the HEA-t and HEA-h alloys are greater than for the HEA alloy. This can be explained by an easier diffusion of Mn when carbides are present in the interdendritic spaces and grain boundaries, or to a faster oxidation of Mn in presence of carbides.

3.6 Assessment of the oxidation kinetics from the metallographic results

These concentration profiles were exploited to deduce the masses of Cr and of Mn lost per surface unit area by the oxidizing alloys. The (1) and (2) formula were used:

$$\frac{m_{Cr}}{S} = \rho_{alloy} \times \int_0^{Ddepth_{Cr}} [f_w^{Cr} - f_w^{Cr}(x)] \times dx \qquad (1)$$

$$\frac{m_{Mn}}{S} = \rho_{alloy} \times \int_0^{Ddepth_{Mn}} [f_w^{Mn} - f_w^{Mn}(x)] \times dx \qquad (2)$$

Where $\frac{m_{Cr}}{S}$ and $\frac{m_{Mn}}{S}$ are respectively the Cr and Mn masses lost, per surface unit area, by the oxidizing alloy, ρ_{alloy} is the volume mass of the alloy (estimated values: 7.9g cm^{-3} for CTR, 8.1g cm^{-3} for HEA-t, and 8.1g cm^{-3} for HEA-h), f_w^{Cr} and f_w^{Mn} are the Cr and Mn weight contents in the initial alloy, $f_w^{Cr}(x)$ and $f_w^{Mn}(x)$ are the current Cr and Mn weight contents in the oxidized alloy at the depth x in the subsurface and $Ddepth_{Cr}$ and $Ddepth_{Mn}$ are the Cr–depleted and Mn–depleted depths respectively.

Assuming that these quantities of Cr and of Mn were oxidized these first results may allow estimating the mass of the formed oxides. Despite that the natures of these ones were multiple, the metallographic results also showed that the $MnCr_2O_4$ and $(Mn,Cr)_3O_4$ species dominate. Further calculations were thus done on the basis of exclusive $(Mn,Cr)_3O_4$ formation, to simplify and for the feasibility of the determination. After having converted the masses per surface unit area into numbers of moles per surface unit area ($\frac{n_{Cr}}{S}$ and $\frac{n_{Mn}}{S}$) using the molar masses of both elements (M_{Cr} and M_{Mn}), according to the (3) and (4) equations, the numbers of oxygen moles and of $(Mn,Cr)_3O_4$ moles per surface unit area ($\frac{n_O}{S}$ and $\frac{n_{(Mn,Cr)_3O_4}}{S}$) were calculated using the (5) and (6) formula. The mass of $(Mn,Cr)_3O_4$ per surface unit area $\frac{m_{(Cr,Mn)_2O_3}}{S}$ was determined from the (7) formula. The oxide mass was finally deduced, according to the (8) formula, in which the value for the oxide density ($\rho_{(Mn,Cr)_3O_4}$) was taken equal to 4.86 g cm^{-3}.

$$\frac{n_{Cr}}{S} = \left[\frac{\frac{m_{Cr}}{S}}{M_{Cr}}\right] \quad (3) \qquad \frac{n_{Mn}}{S} = \left[\frac{\frac{m_{Mn}}{S}}{M_{Mn}}\right] \quad (4)$$

$$\frac{n_O}{S} = \frac{4}{3} \times \left(\frac{n_{Cr}}{S} + \frac{n_{Mn}}{S}\right) \qquad (5)$$

$$\frac{n_{(Mn,Cr)_3O_4}}{S} = \frac{1}{4} \times \frac{n_O}{S} \qquad (6)$$

$$\frac{m_{(Cr,Mn)_2O_3}}{S} = \frac{n_{(Mn,Cr)_3O_4} \times (3 \times (M_{Cr} + M_{Mn}) / 2 + 4 \times M_O)}{S} \qquad (7)$$

$$e_{(Mn,Cr)_3O_4} = \frac{\frac{m_{(Mn,Cr)_3O_4}}{S}}{\rho_{(Mn,Cr)_3O_4}} \qquad (8)$$

Table 3 gathered the results obtained for the masses of Cr and Mn lost by the alloys during oxidation, and the corresponding values of the masses (per surface unit area) and equivalent thicknesses of the $(Mn,Cr)_3O_4$ scales. The 16 to 21 µm of $(Mn,Cr)_3O_4$ thickness for the HEA alloy are a rather lower than suggested by micrographs. This can be explained by

the presence of many pores/voids in the thick outer part of the scale. The agreement is better for the HEA-t and HEA-h alloys.

The total mass gains at the end of the 50 hours of oxidation at 1000°C were estimated by calculating, according to (9), the mass of oxygen gained by the alloys by surface unit area, using the numbers of moles of Cr, Mn and finally O resulting from the (3), (4) and (5) equations above. The parabolic constant Kp was thereafter estimated using equation (10):

$$\frac{m_O}{S} = \frac{n_O}{S} \times M_O \quad (9)$$

$$Kp = \frac{1}{2} \times \frac{\left(\frac{m_O}{S}\right)^2}{50h} \quad (10)$$

The obtained values are displayed in Table 4. The values obtained for the mass gain ("Gained O" column) for the three alloys together are spread out over the [2 mg/cm^2 – 7 mg/cm^2] range which is rather in good agreement with the 4.45 mg/cm^2 earlier found for another equimolar CrMnFeCoNi alloy after oxidation at 1000°C [24]. When one compares directly the oxygen mass gain obtained here for the CTR alloy only, to the 4.45 mg/cm^2 value, it seems that the HEA alloy presents a lower mass gain, taking into account that the oxidation duration in the present work was twice the one for the earlier results (2 to 3 mg/cm^2 here against 4.45 mg/cm^2, for 50 hours here against 24h). This may be a consequence of the differences in alloy synthesis procedure (vacuum induction casting in both cases, but followed by hot rolling followed by homogenization heat treatment in [24], and thus in grain size for instance (here 1 – 2 mm against about 250 µm in [24].

The grain size is effectively of great importance at temperatures close to 1000°C and below, with more intensive intergrain diffusion predominating on volume diffusion when the oxidizing alloy is fine–grained. The values of parabolic constants deduced here (Table 4 too) are spread out over a large interval (13 × 10^{-12} g^2 cm^{-4} s^{-1} to ten times this value). The Kp value obtained at 1000°C for the cast then hot rolled equimolar CrMnFeCoNi [24] was 0.83 mg^2 / cm^4 / h (i.e. 230 × 10^{-12} g^2 cm^{-4} s^{-1}), as is to say rather higher than the values obtained in the present work. One can again evocate the probable effect of the difference in microstructural fineness. By looking to the ranges of Kp values of the HEA, HEA-t and HEA-h alloys, one confirms that the presence of the Ta and Hf reactive elements, and of the corresponding carbides, are harmful for the oxidation resistance of the alloys. The deterioration in oxidation behavior is however rather low for the HEA-t alloy, by comparison with the HEA-h alloy.

4. Conclusion

TaC and HfC are carbides that demonstrated efficient strengthening for the equimolar CoNiFeMnCr high entropy alloy, as shown with recent high temperature creep tests in another study. But it appears that the presence of these carbides induces a more or less dramatic evolution of the oxidation behavior. Among the two types of carbides for reinforcement, only TaC allows high mechanical resistance at elevated temperature without threatening dangerously the oxidation resistance. This one is only a little decreased. Global high performance during high temperature service can be expected with the TaC–strengthened version of the equimolar CoNiFeMnCr HEA alloy.

Table 3. Results of exploitation of the concentration profiles to estimate some parameters characterizing the depletion in chromium and in manganese; corresponding quantities of (M = Mn and/or Cr)$_3$O$_4$ oxide

Depletion characteristics:	Lost Cr (mg/cm^2)	Lost Mn (mg/cm^2)	Corresp^{ding} M_3O_4 mass (mg/cm^2)	Corresp^{ding} M_3O_4 thick^{nss} (µm)
HEA	1 – 2	4 – 5	7.7 – 10.2	16 – 21
HEA-t	1 – 2	5 – 7	8.4 – 11.8	17 – 24
HEA-h	1 – 3	7 – 9	10.6 – 11.4	22 – 49

Table 4. Corresponding values of mass gains and of equivalent parabolic constants

Depletion parameters:	Gained O (mg/cm^2)	Corresp^{ding} Kp values (× 10^{-12} g^2 cm^{-4} s^{-1})
HEA	2.2 – 2.9	13 – 23
HEA-t	2.4 – 3.3	16 – 31
HEA-h	3.0 – 6.8	24 – 127

References

[1] P. Berthod, High temperature properties of several chromium-containing Co-based alloys reinforced by different types of MC carbides (M = Ta, Nb, Hf and/or Zr), Journal of Alloys and Compounds, 481(1–2), (2009) 746-754. [DOI]

[2] S. Michon, L. Aranda, P. Berthod and P. Steinmetz, High temperature evolution of the microstructure of a cast cobalt base superalloy - Consequences on its thermomechanical properties, Revue de Métallurgie, 101(9), (2009) 651-662. [DOI]

[3] P. Berthod, E. Conrath, Creep and oxidation kinetics at 1100 °C of nickel-base alloys reinforced by hafnium carbides, Materials & Design, 104, (2016) 27-36. [DOI]

[4] P. Berthod, E. Conrath, Mechanical and Chemical Properties at High Temperature of {M-25Cr}-based Alloys Containing Hafnium Carbides (M=Co, Ni or Fe): Creep Behavior and Oxidation at 1200°C, *Journal of Material Science and Technology Research*, *1*(1), (2014) 7–14. [DOI]

[5] A. Smekhova, A. Kuzmin, K. Siemensmeyer, R. Abrudan, U. Reinholz, A.G. Buzanich, M. Schneider, G. Laplanche, K.V. Yusenko, Inner relaxations in equiatomic single-phase high-entropy cantor alloy, Journal of Alloys and Compounds, 920, (2022) 165999. [DOI]

[6] B. Cantor, Multicomponent high-entropy Cantor alloys, Progress in Materials Science, 120, (2021) 100754. [DOI]

[7] F.D.C. Garcia Filho, R.O. Ritchie, M.A. Meyers, S.N. Moteiro, Cantor-derived medium-entropy alloys: bridging the gap between traditional metallic and high-entropy alloys, Journal of Materials Research and Technology, 17, (2022) 1868. [DOI]

[8] W.M. Choi, S. Jung, Y.H. Jo, S. Lee, B.J. Lee, Design of new face-centered cubic high entropy alloys by thermodynamic calculation, Metals and Materials International, 23, (2017) 839-847. [DOI]

[9] G. Bracq, M. Laurent-Brocq, L. Perriere, R. pires, J.M. Joubert, I. Guillot, The fcc solid solution stability in the Co-Cr-Fe-Mn-Ni multi-component system, Acta Materialia, 128, (2017) 327-336. [DOI]

[10] S.F. Liu, Y. Wu, H.T. Wang, J.Y. He, J.B. Liu, C.X. Chen, X.J. Liu, H. Wang, Z.P. Lu, Stacking fault energy of face-centered-cubic high entropy alloys, Intermetallics, 93 (2018) 269-273. [DOI]

[11] P. Berthod, As-Cast Microstructures of High Entropy Alloys Designed to Be TaC-Strengthened, Journal of Metallic Material Research, 5(2), (2022) 1–10. [DOI]

[12] P. Berthod, As-cast microstructures of HEA designed to be strengthened by HfC. Journal of Engineering Sciences and Innovation (JESI), 7(3), (2022) 305-314.

[13] H. Song, Q. Ma, W. Zhang, F. Tian, Effects of vacancy on the thermodynamic properties of Co-Cr-Fe-Mn-Ni high-entropy alloys, Journal of Alloys and Compounds, 885, (2021) 160944. [DOI]

[14] J. Sebesta, K. Carva, D. Legut, Evolution of the Curie temperature for a substituted Cantor alloy, PHYSICAL REVIEW B, 103, (2021) 064407. [DOI]

[15] W. Kucza, J. Dabrowa, G. Cieslak, K. Berent, T. Kulik, M. Danielewski, Studies of “sluggish diffusion” effect in Co-Cr-Fe-Mn-Ni, Co-Cr-Fe-Ni and Co-Fe-Mn-Ni high entropy alloys; determination of tracer diffusivities by combinatorial approach Journal of Alloys and Compounds, 731, (2018) 920-928. [DOI]

[16] C. Varvenne, A. Luque, W.A. Curtin, Theory of strengthening in fcc high entropy alloys, Acta Materialia, 118, (2016) 164-176. [DOI]

[17] Z. Zeng, M. Xiang, D. Zhang, J. Shi, W. Wang, X. Tang, W. Tang, Y. Wang, X. Ma, Z. Chen, W. Ma, K. Morita, Journal of Materials Research and Technology, 15, (2021) 1920-1934. [DOI]

[18] P. Berthod, Strengthening Against Creep at Elevated Temperature of HEA Alloys of the CoNiFeMnCr Type Using MC-Carbides, TMS 2023 152nd Annual Meeting & Exhibition Supplemental Proceedings, (2023) 1103-1111.

[19] M. Garg, H.S. Grewal, R.K. Sharma, H.S. Arora, Enhanced Oxidation Resistance of Ultrafine-Grain Microstructure AlCoCrFeNi High Entropy Alloy, ACS Omega, 7, (2022) 12589–12600. [DOI]

[20] M. Esmaily, Y. Qiu, S. Bigdeli, M.B. Venkataraman, A. Allanore, N. Birbilis, High-temperature oxidation behaviour of Al_xFeCrCoNi and AlTiVCr compositionally complex alloys, *npj Materials Degradation,* 4, 25 (2020). [DOI]

[21] L. Wang, Q. Zeng, Z. Xie, Y. Zhang, H. Gao, High Temperature Oxidation Behavior of an Equimolar Cr-Mn-Fe-Co High-Entropy Alloy, Materials, 14(15), (2021) 4259. [DOI]

[22] S. Xia, C.M. Lousada, H. Mao, A.C. Maier, P.A. Korzhavyi, R. Sandström, Y. Wang, Y. Zhang, Nonlinear Oxidation Behavior in Pure Ni and Ni-

Containing Entropic Alloys, Frontiers in Materials, 2018, 5, 53. [DOI]

[23] G. Laplanche, U.F. Volkert, G. Eggeler, E.P. George, Oxidation Behavior of the CrMnFeCoNi High-Entropy Alloy, Oxidation of Metals, 85, (2016) 629-645. [DOI]

[24] Y.K. Kim, Y.A. Joo, H.S. Kim, K.A. Lee, High temperature oxidation behavior of Cr-Mn-Fe-Co-Ni high entropy alloy, Intermetallics, 98, (2018) 45-53. [DOI]

[25] B.L. Pan, M. Wang, Y.G. Shen, X.L. Xi, Z.R. Nie, Improvement in oxidation resistance of Cantor alloy through microstructure tailoring, China Foundry, 19, (2022) 503-510. [DOI]

Conflict of interest

The Author has no conflicts of interest to declare that they are relevant to the content of this article.

Does the Article Screened for Similarity?

Yes.

About the License